Investigation on the Mechanical Performances of Ternary Nylon 6/SEBS Elastomer/Nano-SiO$_2$ Hybrid Composites with Controlled Morphology

Baoqing Zhang,[1*] **Julia Shuk-Ping Wong,**[1] **Dean Shi,**[1,2] **Richard Ching-Man Yam,**[3] **Robert Kwok-Yiu Li**[1]

[1]*Department of Physics and Materials Science, City University of Hong Kong, Tat Chee Avenue, Kowloon, Hong Kong, China*
[2]*Faculty of Materials Science and Engineering, Hubei University, Wuhan 430062, China*
[3]*Department of Manufacturing Engineering and Engineering Management, City University of Hong Kong, Tat Chee Avenue, Kowloon, Hong Kong, China*

ABSTRACT: The distribution of maleated styrene-hydrogenated butadiene-styrene (mSEBS) elastomer and nano-SiO$_2$ in nylon 6 matrix was controlled by varying the blending procedure. Nano-SiO$_2$ particles with different surface properties (hydrophilic versus hydrophobic) were adopted to adjust their interactions with other components. Two different structures, separate dispersion of nano-SiO$_2$ and elastomer particles as well as encapsulation of nano-SiO$_2$ fillers by the elastomer, were obtained. The structures were confirmed through scanning electron microscope (SEM) investigation. The mechanical measurement results showed that the microstructure and the interactions among the components had dramatic influences on the final mechanical properties, especially Izod fracture toughness, for the ternary nanocomposites. The nanocomposites containing hydrophilic nano-SiO$_2$ had better mechanical performances compared with the composites filled with hydrophobic SiO$_2$ when they were in the same microstructure. The nanocomposites with separate dispersion structure showed higher stiffness compared with those of encapsulation type. However, the separately dispersed nano-SiO$_2$ particles restricted the cavitation of elastomer phases that led to low toughening effectiveness. The difference of cavitation intensity for elastomer phase was revealed by SEM investigation on the facture surfaces for the nanocomposites with the two different microstructures. © 2009 Wiley Periodicals, Inc. J Appl Polym Sci 115: 469–479, 2010

Key words: nylon 6; nanocomposites; microstructure; mechanical properties; toughness

INTRODUCTION

The toughening of polymers has been a long time subject of intensive research in industry and academia. Generally, blending with an elastomer is a simple and effective approach to enhance the impact resistance of polymeric matrices, including amorphous and semi-crystalline thermoplastics as well as thermosets.[1] At sufficiently high concentration of elastomeric phase and under favorable conditions, the notched impact strength for the toughened polymer blends can show an improvement of 10 or even several 10-folds.[2–6] With such high impact strength, the material is referred to as "super-tough" polymer. However, the drawback of elastomer-toughening is the resulting significant reduction in the modulus and tensile strength of such blends, and the tensile properties reductions are more severe with the increasing of elastomer content.

An alternative approach to achieve toughening is rigid particle toughening method. Hopefully, improvement of both of the modulus and toughness can be realized at the same time via this approach. Although there are successful examples of effective polymer toughening by using rigid particle inclusions,[7–10] this technique cannot give similar level of toughening as elastomer does.[11] When the dimension of the rigid particle fillers was reduced from micrometer to nanometer scale, the polymer matrices were de-toughened in most cases, especially for nanoclay filled systems.[12–17] It has been widely accepted that for rigid particle toughening, particle/matrix debonding is an important mechanism to trigger the plastic deformation of matrix, which leads to improved fracture toughness.[9,10] The easy debonding means weak particle-matrix adhesion. However, to fulfill the reinforcing effect of micro- or nano-rigid particles, it is necessary to improve their dispersion and hence better interaction with the polymer matrix. So the interphase

between polymer and rigid particles needs to be specifically designed to achieve reinforcing and toughening simultaneously by using this approach.[13,18–20]

Over the last several decades, many publications have appeared that deal with the simultaneous reinforcing and toughening of polymer/elastomer/rigid-filler ternary composites.[21–32] For such ternary composites, two types of distinctive structures can be obtained: (1) separate dispersion of fillers and elastomer particles; (2) encapsulation of fillers by the elastomer phase (also called core-shell structure). Generally, the final structure is mainly controlled by thermodynamic parameters (such as the interfacial tension, adhesion work) and other potential physical or chemical interactions between the components. In addition, processing parameter settings such as blending sequences, blending time, and blending strength will also produce significance influences on the final phase structure. This is due to the difficulty in reaching the stable thermodynamic state during melt blending. By controlling the above mentioned parameters, well-defined phase structures in polymer/elastomer/rigid-filler ternary composites can be produced. At the moment, it is still controversial as to which structure is beneficial for reinforcing and toughening. In the simulation study carried out by Matonis and Small,[21] it was suggested that for rubber coated rigid particulate filled polymer, the relative rubber thickness to core-shell particle radius needed to be >0.04 to provide sufficient toughening effect. However, such rubber coated rigid particulate inclusions could not improve the stiffness of the matrix. Similar to this simulation result, the majority of experimental studies have shown that the separate dispersion structure is favorable for reinforcing while the encapsulation structure is favorable for toughening. But there also exist other opinions. Jancar et al.[23] showed that ternary composites with the core-shell structure possessed higher tensile impact strength; the core-shell inclusions were less effective as toughening agent when compared with the unreinforced elastomer itself. The results presented by Stricker et al.[24] indicated that on comparing the separate dispersion structure and the core-shell structure, the former was more positive to enhance both the stiffness and toughness of ternary composites. Premphet et al.[25] also found that the composites with separate dispersion structure showed higher modulus and impact strength than those of the composites with core-shell type morphology. However, to obtain the desired structures, two elastomers with different polarity and different toughening effect on the matrix had been used.[25] Recently, Fu et al.[33] carried out a detailed investigation on the morphology and toughening phenomenon in polypropylene (PP)/elastomer/nano-SiO$_2$ ternary system. In their study, a unique structure consisting of

elastomer particles surrounded by SiO$_2$ agglomerations was observed, which showed dramatically better toughening effect than that of separate dispersion or core-shell structure. They ascribed this result to the overlapping of the stress volumes between soft and rigid particles.[33] Without doubt, their finding is novel and interesting. But their method is hard to be extended to other systems because the formation of the observed unique structure is a kinetics controlled process, which is strongly affected by the processing time of the second blending step.[34]

Due to the de-toughening effect commonly observed in polymer/clay nanocomposites, there have been active research studies on blending of elastomer with these nanocomposites.[35–41] However, little attention has been paid on the interrelationship between phase structure and toughness/stiffness in these materials. In general, the polymer/elastomer/clay nanocomposites were mainly prepared by either one-step (all components were blended simultaneously) or two-step compounding method (polymer/clay were blended first and the mixture was further blended with elastomer later). By adopting the appropriate blending method, well separated dispersion of clay nano-layers and elastomer particles could be obtained. Ahn and Paul[41] claimed that the hybrid nanocomposite with such phase structure was desirable for the optimal stiffness-toughness balance. Chiu et al.[37] noticed that the ternary composites prepared by using different blending sequences had variations in mechanical performances, but the detail investigations on the phase structures and explanations for the properties differences have not been given. It appeared that the research carried out by Dasari et al.[35,38] was the only work that gave a detail characterization on the relationship between the fracture performance and the microstructure of ternary nylon/elastomer/clay nanocomposites, with the different microstructures obtained from using different blending sequences. Their results showed that the ternary nanocomposite with an encapsulation structure possessed the lowest impact strength. So they also suggested that the separate dispersion of clay and elastomer phase was preferred for a better combination of toughness, strength, and stiffness. But the elastomer content in their investigated systems was fixed at 15 wt %. It is questionable that the microstructure-performance correlation that they suggested is still tenable when the elastomer content is higher than 15 wt %, for example, 20 wt %, after the brittle-to-ductile transition occurs.

Polypropylene (PP) has been frequently used as the polymer matrix in most of the researches that concerning polymer/elastomer/filler systems. However, PP is a nonpolar polymer. To gain a better picture on the toughening of ternary blends with polar matrices, it would be of interest to use a nylon as

the matrix. In addition, nylon has been widely used to prepare polymer/clay nanocomposites nowadays. Spherical nanoparticles, which are isotropic and regular shaped, will be ideal model fillers for the understanding of the interaction between rigid-filler, elastomer and polymer. Based on these reasoning, ternary composites consisting of nylon 6, functionalized elastomer and nano-SiO$_2$ with different surface properties (hydrophilic and hydrophobic) were prepared in this research. The above components were melt-blended by using different blending procedures. The objectives of the present study are:

- to investigate the effects of nano-particle surface characteristics and blending procedures on the microstructure development in the ternary blends;
- to study the correlation between microstructure and mechanical performance for the ternary blends, especially their impact resistance in standard Izod impact test.

EXPERIMENTAL

Materials and preparation

The nylon 6 (PA6) used in this study was supplied by DuPont Company (grade Zytel 7331J NC010). The toughening rubber used was a maleic anhydride (MA) grafted styrene/ethylene/butadiene/styrene triblock copolymer, which was supplied by Shell Chemical Company (grade Kraton FG1901X). This functionalized rubber will be referred to as mSEBS in this article. The MA content of the Kraton FG1901X is 1.84 wt % according to published literature.[42]

Two types of nano-sized fumed silica were used in this work, and both were obtained from Degussa Co., Germany. The first one is Aerosil 200 (which will be referred to as Silica-A in this work), which is a hydrophilic silica due to its fully hydroxylated surface. The second one is Aerosil R974 (which will be referred to as Silica-B), which is a hydrophobic silica. Silica-B has been pretreated with 1,1-dimethyl-dichlorosilane in the supplied form. The detail phys-

icochemical properties of the two kinds of nano-SiO$_2$ are listed in Table I.[43]

Before melt processing, PA6, mSEBS, and silica powders were dried in air-circulating ovens at 90, 60, and 105°C, respectively, for about 12 h. Two different processing procedures were used in preparing the PA6/mSEBS/nano-SiO$_2$ ternary composites.

Procedure I

The mSEBS pellets and nano-silica powder were firstly mixed in a Brabender internal-mixer at 170°C for about 8 min. Despite that Silica-A and Silica-B had different surface properties, they were both homogeneously dispersed into mSEBS. This can be seen from the similar level of transparencies for the plaques obtained from unfilled mSEBS, mSEBS/Silica-A, and mSEBS/Silica-B (photograph not shown here). The mSEBS/silica homogeneous mixtures were melting blended with PA6 matrix by using a Brabender twin-screw extruder with the barrel temperatures at the range of 230–245°C. The weight ratio of the different components in the ternary nanocomposites was fixed at PA6/mSEBS/silica = 76/19/5. Neat PA6 and PA6/mSEBS (80/20 wt %) binary blend were also extruded at the same conditions for further injection moulding and testing.

Procedure II

PA6/Silica-A and PA6/Silica-B master-batches with silica content of about 10 wt % were first prepared in a Haake TW100 twin-screw extruder. Then the master-batches were blended either with only PA6 or with both PA6 and mSEBS to obtain PA6/silica binary and PA6/mSEBS/silica ternary composites with the desired composition.

After pelletizing and drying, the obtained materials were injection-moulded into standard tensile bars by using a COSMO TTI-220/80 injection-moulding machine (Welltec Industrial Equipment, Hong Kong). The injection temperatures from the hopper to the injection nozzle were set at the range of 240–255°C.

Summaries of the different blend designations and compositions are shown in Table II.

TABLE I
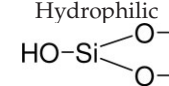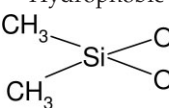Physicochemical Properties of nano-silicas Used in this Study[44]

Physical properties	Density (g/cm^3)	BET surface Area (m^2/g)	Average primary particle diameter (nm)	Surface property	Purity (wt % of silica)
Aerosil 200 (Silica-A)	2.2	200 ± 25	12	Hydrophilic $HO-Si {<}^{O-}_{O-}$	≥ 99.8
Aerosil R974 (Silica-B)	2.0	170 ± 20	12	Hydrophobic $^{CH_3}_{CH_3} {>} Si {<}^{O-}_{O-}$	≥ 99.8

TABLE II
Interpretation of Sample Code for the Materials Investigated in this Work

Code	Composition (weight ratio)				Preparing procedure
	PA6	mSEBS	Silica-A	Silica-B	
PA6	100	—	—	—	—
PA6/mSEBS	80	20	—	—	—
PA6/Silica-A	95	—	5	—	Dilution from master-batch
PA6/Silica-B	95	—	—	5	Dilution from master-batch
AI	76	19	5	—	I
BI	76	19	—	5	I
AII	76	19	5	—	II
BII	76	19	—	5	II

Differential scanning calorimetry (DSC)

DSC analysis was carried out with a TA 2920 modulated DSC system. The test samples (7–10 mg) were cut from the middle section of tensile specimens. Each sample was first heated from 30 to 250°C at a rate of 10°C/min and maintained at 250°C for a period of 5 min, then cooled down to 30°C at the same rate, after that heated again from 30 to 250°C with a rate of 10°C/min. The crystallization temperature T_c, and melting temperature T_m, were obtained from the cooling and the second heating scans. The recorded heat of fusion was used to calculate the level of crystallinity by dividing it with the heat of fusion of the purely crystalline forms of nylon 6, i.e., 240 J/g.[44]

Mechanical testing

Tensile tests were carried out by using an Instron model 5567 universal testing machine at room temperature. The tensile modulus of the samples was measured at the crosshead speed of 1 mm/min. A clip-on extensometer (25 mm gauge length) was used to measure the tensile strain to give accurate measurement of the tensile Young's modulus. Other tensile properties were measured at the speed of 20 mm/min by measuring simultaneously of the load and strain. An extensometer (50 mm gauge length) with high extensibility was used to accurately measure the tensile strain till the rupture of the specimen. The average value of at least five tests was reported.

Notched Izod impact tests were carried out by using a Ceast 6545 pendulum impact tester according to ASTM D256. As in the tensile test, a minimum of five specimens were tested and the result reported.

Morphology observation

To investigate the dispersion of nano-silica particles and measure the size distribution of dispersed mSEBS phase, some tensile specimens of the ternary composites were cryogenically fractured in liquid nitrogen, and the fractured surfaces were etched with hot toluene vapour for 12 h to remove the dispersed mSEBS phase. After coated with gold, the etched samples were observed with a JOEL JSM 6335 field-emission scanning electron microscope (SEM) at an acceleration voltage of 5 kV. The diameters of mSEBS particles were measured from SEM photos by using an image analysis software (Scion Image 4.0, Scion Corporation). For each sample, the diameters for at least 400 mSEBS particles were measured and the average diameter calculated.

The broken samples after Izod impact test were also characterized by optical and SEM investigations. Optical microscopic investigation was carried out on an Olympus SZX stereo microscope equipped with a Nikon DS-Fi1 digital camera. SEM investigations were performed on a JOEL JSM 820 SEM at an acceleration voltage of 20 kV. Before SEM observations, the impact fracture surfaces were also coated with a gold layer to avoid charging problem.

RESULTS AND DISCUSSIONS

Morphological investigation

SEM investigation

SEM micrographs showing the cryogenic fractured surfaces of the different ternary composites (i.e., PA6/mSEBS/nano-SiO$_2$) after solvent-etching are shown in Figure 1. The holes on the surface correspond to the mSEBS phase which had been selectively removed by toluene vapor, whereas the bright particles are silica nanofiller. It can be seen that some of the silica particles form aggregates as their sizes are bigger than the primary diameter of nano-silica particle (i.e., 12 nm).

From the SEM micrographs shown in Figure 1, it can be seen that by adopting two different blending procedures, distinctly different microstructures and distributions of SiO$_2$ can be obtained in the ternary composites. As shown in Figure 1(a,c), when the nano-SiO$_2$ was first blended with mSEBS and then the mSEBS/SiO$_2$ mixture was blended with PA6 (i.e., Procedure I), the ternary nanocomposites have the core-shell morphology in which the nano-SiO$_2$ particles were encapsulate by mSEBS phase. This is
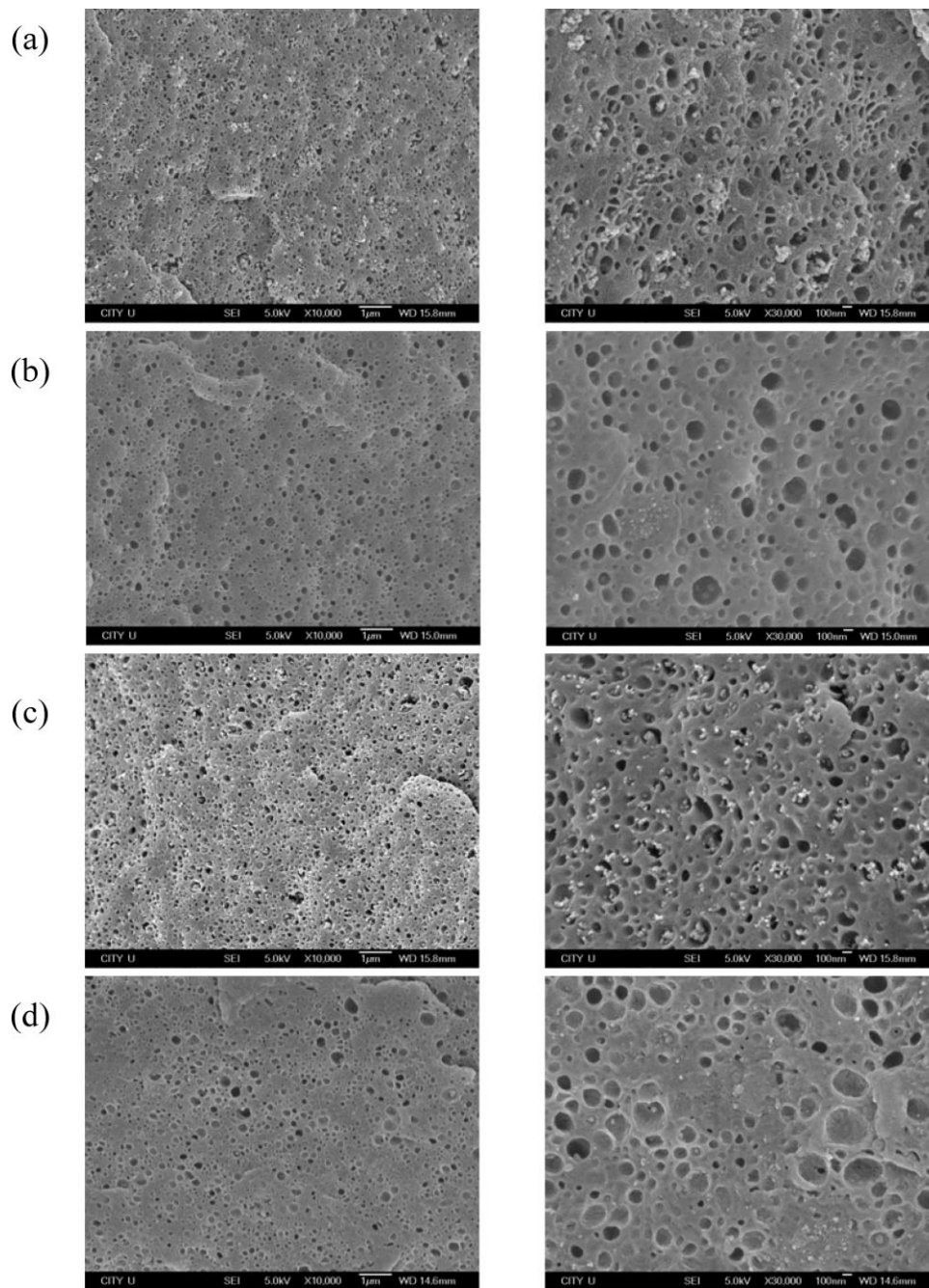
Figure 1 SEM images of PA6/mSEBS/silica [76/19/5 (wt/wt %)] ternary nanocomposites at the magnification of ×10,000 (left column) and ×30,000(right column): (a) AI, (b) AII, (c) BI, and (d) BII.

inferred from the observation that throughout the fracture surfaces, most of the SiO_2 aggregates can be seen as the residue in the dark holes left after the mSEBS phase being extracted. It should be pointed out that the complete encapsulation has not been achieved as some SiO_2 particles can be seen in PA6 matrix no matter whether Silica-A or Silica-B was used. When a different blending procedure was applied (i.e., Procedure II), the different morphology was obtained in which mSEBS and silica particles were separately dispersed in PA6 matrix. That is

supported by the SEM pictures shown as Figure 1(b,d). In these figures, all the silica particles are still embedded in the PA6 matrix and no isolated particles or aggregates can be found in the holes left by the extracted mSEBS.

The size distributions of the mSEBS particles were measured from the SEM photographs for a further quantitative analysis. According to Wu's theory,[45,46] for elastomer toughened polymer blends, there is a certain critical matrix ligament thickness (τ_c) that below which a sharp brittle-to-tough transition
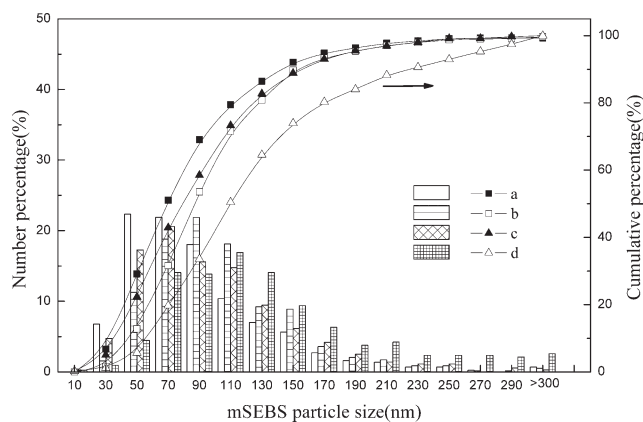
Figure 2 Distribution of mSEBS particle size in PA6/mSEBS/silica ternary nanocomposites: (a) AI, (b) AII, (c) BI, and (d) BII.

occurs. The matrix ligament thickness (τ) correlates to the elastomer volume fraction (φ_e) by[46]:

$$\tau = d[(\pi/6\phi_e)^{1/3} - 1], \tag{1}$$

where d is the elastomer particle diameter. For nylon matrix, the critical matrix ligament thickness commonly falls into the range of about 0.2–0.3 μm at room temperature.[46,47] The size distributions of mSEBS particles in the four different types of PA6/mSEBS/silica ternary composites are shown in Figure 2. Based on these measurements, the number-average diameter for mSEBS particles and the corresponding matrix ligament thickness in the ternary nanocomposites calculated from eq. (1) are summarized in Table III. To calculate the volume fraction of each phase, the density for PA6, mSEBS, Silica-A, and Silica-B were taken to be 1.14, 0.91, 2.2, and 2.0 g/cm^3, respectively. Moreover, the total volume fraction of mSEBS and silica was taken as that of elastomer phase when an encapsulation microstructure was formed by utilizing Procedure I. As can be seen from Table III, the mSEBS particles in all the systems are relatively small, which means that the compatibility between mSEBS and PA6 was greatly enhanced by the *in-situ* formed copolymer derived from the reaction of MA group of mSEBS with the terminal amino group of PA6.[3] Therefore, the corresponding matrix ligament thickness, τ, in each ternary nanocomposite is also far below the commonly accepted critical τ value for PA6 (i.e., about 0.2–0.3 μm).

Another interesting but unexpected observation is that the elastomer particles in the systems with separate dispersion structure are somewhat larger compared with those in the composites with encapsulation structure. As commonly accepted, PA6 filled with nanoparticles possesses a higher viscosity that leads to a higher shear stress during melt-blending and so a smaller dispersed elastomer particle size.

Whereas the dispersed phase with high viscosity, namely, the nano-SiO$_2$ filled mSEBS used here, results in a bigger dispersed particle size. The increased viscosities were confirmed from the increased blending torque measured during the preparation of PA6/nano-SiO$_2$ master-batches and mSEBS/nano-SiO$_2$ blends. Both Paul et al.[41] and Nazabal et al.[39] presented the results in organic-montmorillonite (OMMT) filled PA6/mSEBS blends that the elastomer particles sizes in PA6 ternary nanocomposites were clearly larger than those in their corresponding PA6/mSEBS blends. In the systems they investigated, mSEBS and OMMT dispersed separately in PA6 matrix just as the microstructure in our systems that prepared via Procedure II. Nazabal et al.[39] ascribed this to the reason that the intercalated surfactant of OMMT could interact with the maleic groups of mSEBS, and hence obstruct the reaction of PA6 and mSEBS, and thus suppress the compatibility between them. Undoubtedly, the results observed here were also caused by the decreased compatibility between PA6 and mSEBS when the separate dispersion structure formed. However, the reason proposed by Nazabal et al.[39] cannot be used to explain the observation in our study: the increase of particles size (Table III) is more obvious in the systems filled with Silica-B (the hydrophobic one), which has little interaction effect with the functional group of mSEBS. Most probably, the inhibition of the reaction between PA6 and mSEBS was caused mainly by the physical coverage effect of nano-silica at the interphase between mSEBS particles and PA6 matrix. This is similar to the case in a polycarbonate (PC)/thermotropic liquid crystalline polymer (TLCP) blend presented by Wu et al.[48]. In their investigations, the transesterification reaction between PC and TLCP was greatly depressed by the added nano-SiO$_2$, which showed the tendency to locate at the interphase between PC and TLCP. As in the systems studied here, the hydrophobic SiO$_2$ particles have the low miscibility with both PA6 and mSEBS, so they have more tendencies to transfer to the interphase between PA6 and mSEBS compared with the hydrophilic ones. Thus, it is understandable why the increase of

TABLE III
Numer-Average Diameter (d) for mSEBS Particles, Corresponding Matrix Ligament Thickness (τ) and the Increment Ratio of Dispersed mSEBS Particles Size in the Ternary Nanocomposites Prepared with the Blending Procedures I and II

	Procedure I		Procedure II		
Systems	d (nm)	τ (nm)	d (nm)	τ (nm)	Δd^a (%)
PA6/mSEBS/Silica-A	90	24	106	34	13.3
PA6/mSEBS/Silica-B	99	26	137	43	38.4

^{a} $\Delta d = [d(\text{Proc.II}) - d(\text{Proc.I})]/d \, (\text{Proc.I}) \times 100\%$

TABLE IV
Summarization of the Data Obtained from DSC Test

Systems	T_m (°C)	X (%)	$T_{c,onset}$ (°C)	T_c (°C)
PA6	223.9	31.1	185.8	181.4
PA6/mSEBS	221.9	26.4	184.0	178.3
PA6/Silica-A	222.8	28.8	187.1	183.7
PA6/Silica-B	222.5	30.2	188.2	184.5
AI	223.5	26.2	183.6	177.3
BI	223.7	28.4	182.6	178.0
AII	223.0	27.7	187.9	183.2
BII	221.3	26.1	186.7	182.2

particles size is more obvious in the composites containing hydrophobic nano-silica particles.

DSC investigations

In addition to SEM investigation, DSC technique was commonly used as a complementary method for the investigation of phase structure in multiphase composites.[31,32] Table IV shows the various parameters obtained from DSC test for the investigated materials.

Compared with the changes of melting temperature (T_m), onset ($T_{c,onset}$), and peak crystallization temperature (T_c) values for the systems presented by Preechachon et al.[31] and Li et al.,[32] the variations of these parameters are relatively small in our study. So the DSC result presented in Table IV cannot be used as a direct evidence to confirm the phase structure.

However, it is undoubted that the perfection degree of PA6 crystalline lamellae is lowered by the incorporation of elastomer or nano-silica, because the T_m and crystalline degree (X_c) of PA6 in the binary blends decrease slightly after the incorporation of mSEBS or silica. The decrease of X_c also exists in the ternary nanocomposites when mSEBS and SiO_2 fillers are added together. But the small differences of X_c among the filled systems, especially for the ternary nanocomposites, indicate that the X_c difference is not a decisive factor for the mechanical property differences of the final materials.

It can be concluded that the microstructures of PA6/mSEBS/nano-SiO_2 composites have been successfully controlled by employing appropriate blending procedures. Two distinctly different types of microstructures, namely (i) encapsulation of nano-SiO_2 fillers by elastomer phase, and (ii) separate dispersion of fillers and elastomer particles have been obtained in the ternary nanocomposites irrespective of whether the silica surface is hydrophilic or hydrophobic. However, there are some slight differences in the nanocomposites with the same type of structure but containing nanoparticles with different surface properties. When nano-silica and mSEBS particles are separately dispersed in the PA6 matrix, the hydrophobic silica (Silica-B) has a stronger tend-

ency to locate at the interface between mSEBS and PA6, which can be ascribed to its low miscibility with both PA6 and mSEBS phase.

Mechanical properties

Figure 3 shows the typical stress-strain curves for PA6/mSEBS blend, and PA6/mSEBS/silica ternary nanocomposites prepared by adopting the two blending procedures. For all the investigated systems, the mechanical data obtained from the tensile measurement, and the Izod impact strength are summarized in Table V.

In our preliminary experiment on the Izod impact strength of PA6/mSEBS binary blends, it has been observed that a sharp brittle-to-ductile transition occurred at about 15 wt % of mSEBS content. Therefore, in this study, the mSEBS content in PA6/mSEBS was selected to be 20 wt %, and a supertoughened blend with the Izod impact strength of 1033 ± 33 J/m was obtained. However, both the tensile strength and Young's modulus of this blend decrease when comparing to those of PA6 (Table V). On the contrary, the addition of nano-silica particles tends to increase the stiffness of PA6. And the PA6/Silica-A binary nanocomposite has a higher Young's modulus than that of PA6/Silica-B nanocomposite. It is believed that Silica-A, with hydroxyl groups on its surface, has possible physical or chemical interaction with nylon molecular chains, thus displays a better miscibility than that of Silica-B with PA6.

In the ternary nanocomposites, the surface characteristic of the nanoparticles also has dramatic influences on the mechanical performances. Compared with the tensile strength of PA6/mSEBS binary blend, the incorporation of nano-SiO_2 causes a slight increase of tensile strength regardless of the surface
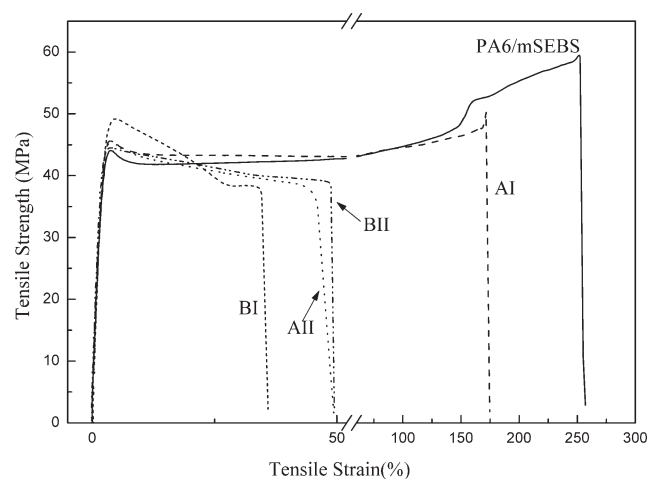

Figure 3 Typical stress-strain curves of PA6/mSEBS blend, PA6/mSEBS/silica ternary composites filled with Silica-A or Silica-B that prepared by using Procedure I and II, respectively.

TABLE V
Mechanical Properties of Investigated Materials

Materials	Maximum tensile strength (MPa)	Young's modulus (GPa)	Elongation at break (%)	Izod impact strength (J/m)
PA6	67.3 ± 0.8	2.62 ± 0.11	57.1 ± 12.2	63.7 ± 6.6
PA6/mSEBS	43.9 ± 0.5	1.90 ± 0.03	235 ± 23	1033 ± 33
PA6/Silica-A	62.9 ± 3.0	3.23 ± 0.09	6.6 ± 0.5	25.9 ± 4.9
PA6/Silica-B	50.9 ± 0.8	3.03 ± 0.02	1.2 ± 0.4	20.1 ± 8.9
AI	44.2 ± 1.2	2.06 ± 0.03	172 ± 12	1230 ± 40
BI	49.2 ± 0.1	1.98 ± 0.03	36.7 ± 6.1	611 ± 6
AII	45.2 ± 0.3	2.29 ± 0.08	41.3 ± 4.3	323 ± 12
BII	44.5 ± 0.8	2.09 ± 0.04	47.7 ± 5.1	231 ± 13

characteristic of nanoparticles and the phase structure. Blending PA6/mSEBS with nano-SiO$_2$ causes a decrease of elongation at break, but the decrease is the least for AI (with an encapsulation structure). In fact, this system shows a very ductile behaviour during tensile test, which can be seen from the stress-strain curve shown in Figure 3. The decrease of elongation at break for the other ternary nanocomposites (i.e., AII, BI, and BII) is more pronounced, but these values are still bigger than those for PA6/nano-SiO$_2$ binary composites. These ternary nanocomposites show a semi-ductile behavior during tensile test.

The addition of nano-SiO$_2$ also contributes noticeably to the Young's modulus of PA6/mSEBS blend. At the same time, the difference of modulus between the four ternary nanocomposites is evident. Generally, formation of separate dispersion structure and using of hydrophilic Silica-A are more effective to increase the stiffness of ternary composites. To further illuminate the effects of phase structure and particle surface property on composite modulus, the Halpin–Tsai equation is applied to calculate the modulus for the silica filled binary and ternary systems. The Halpin–Tsai equation is expressed as[49]:

$$E_c = E_m \frac{1 + \alpha\beta\phi_f}{1 - \beta\phi_f} \qquad (2)$$

where E_c and E_m are the modulus of the composite and the matrix, respectively; ϕ_f is the volume fraction of the particle filler; α is a parameter characterizing the reinforcement shape and distribution, which is equal to 2 for spherical particles; β is a coefficient given by:

$$\beta = \frac{m - 1}{m + \alpha} \qquad (3)$$

in which $m = E_f/E_m$ and E_f is the modulus of SiO$_2$ (taken as 72 GPa here). The experimental obtained modulus data of PA6 and PA6/mSEBS (80/20) blend were used as matrix values for the binary and ternary phase systems, respectively. For ternary composites, calculating in this way means there is no interaction between the solid fillers and elastomer

particles and they act independently in PA6 matrix. This is a close approximation to the ternary composites that have the separate dispersion structure. The calculation results are presented in Figure 4. For both PA6/Silica-A and PA6/Silica-B binary nanocomposites, the experimental measured Young's moduli are higher than the Halpin–Tsai calculations. This can be ascribed to the large specific area of nanoparticles that makes them more effective for reinforcing purpose. For the ternary nanocomposites, two different situations exist. For AI and BI systems, in which the phase morphology for the composites is of an encapsulation structure, the experimental obtained modulus is very close (for AI) or slightly lower (for BI) than the predicted value. On the contrary, for AII and BII ternary nanocomposites, where nano-SiO$_2$ and mSEBS particles are separately dispersed in the PA6 matrix, they possess higher Young's modulus than the predicted values. And the Young's modulus for AII is also higher than that of BII. These results suggested that in the investigated systems, the separate dispersion structure
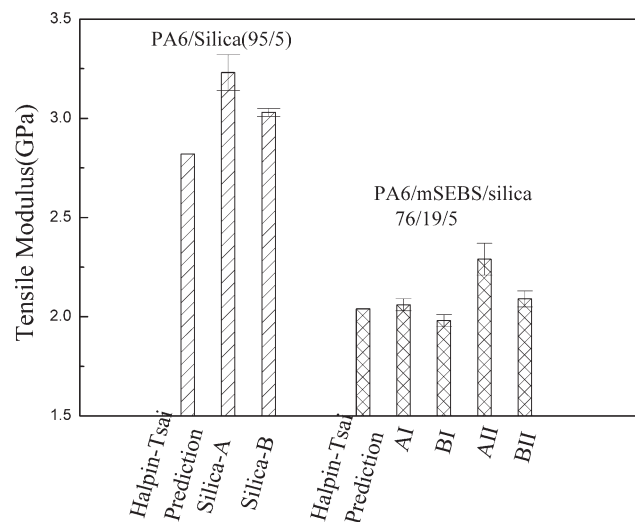

Figure 4 Comparison of the Young's modulus predicted by Halpin-Tsai equation with experimental results for PA6/silica binary and PA6/mSEBS/silica ternary nanocomposites.

favors the reinforcing effect of nano-fillers. Furthermore, a good interfacial interaction between nano-fillers and matrix is preferred for good reinforcing efficiency.

The Izod impact strengths for all the investigated systems are reported in Table V. It can be seen that the impact strength differed significantly for the ternary nanocomposites. When Silica-A was used and an encapsulation structure formed in the ternary nanocomposites (system AI), it presents a high impact toughness that is even higher than that of PA6/mSEBS binary blend (1230 $\pm$ 40 J/m vs. 1033 $\pm$ 33 J/m). This is contrary to the result of Dasari et al.[38] that the ternary PA66/mSEBS/OMMT nanocomposite with an encapsulation structure showed the lowest impact strength.

Considering the higher toughness of the ternary nanocomposite AI than that of the PA6/mSEBS blend, it cannot be simply ascribed to the reason that the volume of elastomer phase is increased by the inclusion of the nanoparticles.[50] The result presented by Nazabal et al. indicated that the Izod impact toughness of PA6/mSEBS blends changed little after brittle-to-ductile transition occurred.[39] Our preliminary experiment also confirmed this. In a PP/ethylene-propylene-diene elastomer (EPDM)/nano-CaCO$_3$ ternary composites, Wang et al.[51] suggested that the debonding between nano-CaCO$_3$ and EPDM as well as the deformation of nano-CaCO$_3$ agglomerates could dissipate the impact energy and resulted in the excellent toughness property for the ternary nanocomposites with the encapsulation structure. By considering the two ternary systems with encapsulation structure in the present investigation, AI and BI, the above proposed debonding and deformation phenomena are more likely to occur in the composite containing Silica-B (BI). Because it had been surface treated and so had a low miscibility with mSEBS and also low aggregation strength between themselves. However, the ternary nanocomposite BI showed lower impact strength than that of AI (611 $\pm$ 6 J/m vs. 1230 $\pm$ 40 J/m). This indicates that the mechanism suggested by Wang et al.[51] is also not applicable in our investigated systems.

It is believed that the cavitation induced matrix shear yielding is still the main toughening mechanism in AI and BI systems, as their entire fracture surface and certain volume of subsurface material were whitened after the fracture test [Fig. 5(a)]. In this figure, both the visible shear lips and the lateral contraction of the sample indicate a high impact toughness of AI.[52] Compared with that of neat mSEBS, mSEBS/SiO$_2$ mixtures have higher moduli. When they disperse in PA6 matrix as the so-called "core-shell" encapsulation particles, they are easier to cavitate than neat mSEBS particles because the elastomer particles with higher bulk modulus endure the larger hydrostatic tension inside them, which makes them easier to cavitate.[53] Bear in mind that the prerequisite
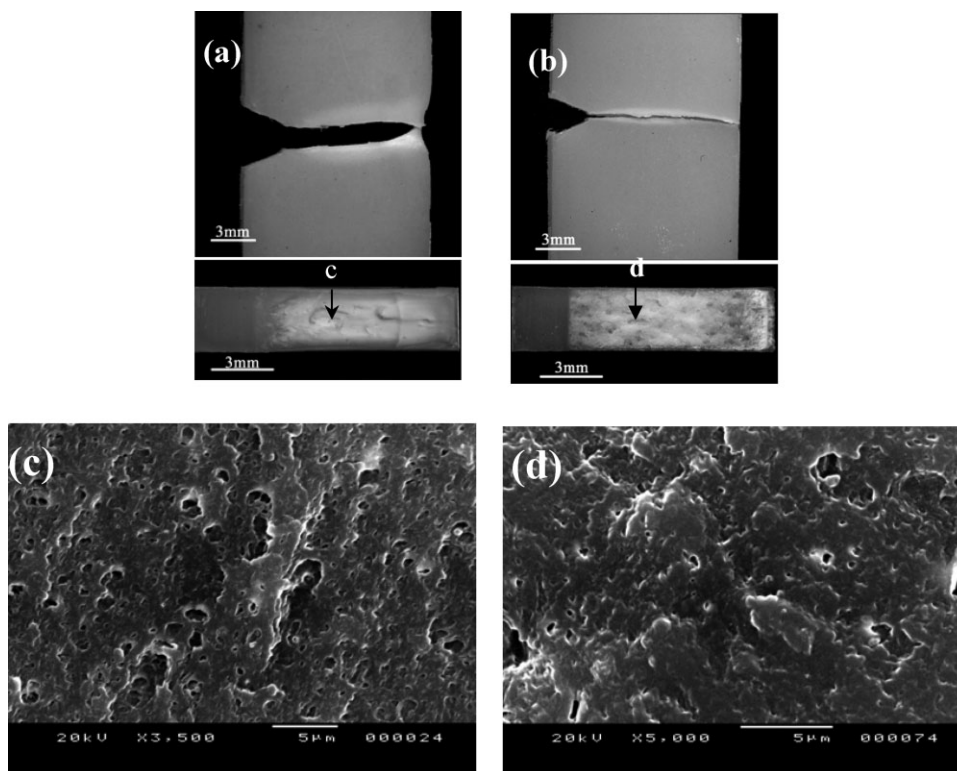

Figure 5 Optical and SEM micrographs of postfracture samples for AI (a, c) and AII (b, d). The arrows in figures (a) and (b) indicate the investigated locations where SEM micrographs (c) and (d) were obtained, respectively.

is the filling of rigid particles do not seriously restrict the elastomer's cavitation ability. The cavitation of mSEBS would release the triaxial stress ahead of the crack-tip and cause the shear yielding of PA6 matrix. The dramatically different toughness between AI and BI might arise from the different behaviours after the initiation of shear yielding. Though the stress-strain curves shown in Figure 3 were obtained in the tensile test, they still give a hint about the limited extent of postyielding deformation for BI in the fracture loading condition. The limited deformation of BI would cause the localized shear yield deformation and limit the energy absorbed in the fracture process.[54] Thus, BI shows a lower Izod impact strength, which is only about the half of AI.

In the cases of ternary nanocomposites AII and BII, when elastomer and SiO_2 nanoparticles formed separate dispersion structure, mSEBS was not so effective to toughen PA6 matrix as itself in AI and BI systems. Here, the reason of size difference of elastomer particles, which was caused by adopting different blending procedures, could be excluded, because the matrix ligament thickness τ in AII and BII (Table III) was still far below the critical matrix ligament thickness τ_c of PA (0.2–0.3 μm typically). Most probably, the stress concentration around the SiO_2 particles hindered the cavitation of elastomer for the stress-whitening volume in their fracture samples was limited compared with those of samples AI and BI [Fig. 5(a,b)]. SEM observation of the fracture surfaces for AI and AII, shown in Figure 5(c,d), reveals a notable difference of cavitaion intensity for mSEBS particles in these two materials. A similar situation exists for the ternary composites containing Silica-B, i.e., BI and BII [Figures not shown here]. These results support the opinion that the toughening effect of elastomer in the ternary composites is mainly controlled by its cavitation ability, which is further controlled by the relative contents, spatial distributions and interactions between the rigid nano-fillers and elastomer phase. It can be concluded briefly that the ternary nanocomposites with encapsulation structure and a good interfacial adhesion between nano-fillers and elastomer phase are preferred for the large improvement of toughness.

CONCLUSIONS

For the investigated PA6/mSEBS/SiO_2 nanocomposites, two typical structures, separate dispersion structure and encapsulation structure, were obtained by adopting two different blending procedures. The final structure of the ternary nanocomposite was mainly controlled by the blending sequence. The surface characterization of SiO_2 showed limited influences on the fine morphology. However, the mechanical performances of the ternary nanocomposites were influenced by both the morphology and the interfacial interactions between the components. Generally, the composites containing hydrophilic nano-SiO_2 had better mechanical performances than the corresponding composites in the same morphology but filled with hydrophobic SiO_2. The nanocomposites with separate dispersion structure showed higher modulus but relatively lower impact strength compared with those of encapsulation type. In our investigated systems, the extensive shield yielding of the nylon matrix, which triggered by the cavitation of mSEBS particles, was corresponding for the large improvement of impact toughness. Optical microscopy and SEM investigations on the fracture surface revealed that there were big differences of cavitation intensities between the nanocomposites with different microstructures and so the notable differences of toughness between them.

For the PA6/mSEBS/SiO_2 systems investigated here, it is difficult to say that which structure is preferable for the optimal stiffness-toughness balance, especially when considering the dramatic differences of Izod impact strengths between the composites with different structures. In real application, it is depends on which properties is more concerned, stiffness or toughness, to decide which morphology should be adopted.

References

1. Collyer, A. A., Ed. Rubber Toughened Engineering Plastics; Chapman & Hall: London, 1994.
2. Yee, A. F.; Pearson, R. A. J Mater Sci 1986, 21, 2462.
3. Oshinski, A. J.; Keskkula, H.; Paul, D. R. Polymer 1992, 33, 268.
4. Huang, D. D.; Wood, B. A.; Flexman, E. A. Adv Mater 1998, 10, 1207.
5. Wilkinson, A. N.; Laugel, L.; Clemens, M. L.; Harding, V. M.; Marin, M. Polymer 1999, 40, 4971.
6. Yu, Z. Z.; Ke, Y. C.; Ou, Y. C.; Hu, G. H. J Appl Polym Sci 2000, 76, 1285.
7. Bartczak, Z.; Argon, A. S.; Cohen, R. E.; Weinberg, M. Polymer 1999, 40, 2347.
8. Chan, C. M.; Wu, J. S.; Li, J. X.; Cheung, Y. K. Polymer 2002, 43, 2981.
9. Zuiderduin, W. C. J.; Westzaan, C.; Huetink, J.; Gaymans, R. J. Polymer 2003, 44, 261.
10. Thio, Y. S.; Argon, A. S.; Cohen, R. E. Polymer 2004, 45, 3139.
11. Wilbrink, M. W. L.; Argon, A. S.; Cohen, R. E.; Weinberg, M. Polymer 2001, 42, 10155.
12. Reynaud, E.; Jouen, T.; Gauthier, C.; Vigier, G.; Varlet, J. Polymer 2001, 42, 8759.
13. Lazzeri, A.; Zebarjad, S. M.; Pracella, M.; Cavalier, K.; Rosa, R. Polymer 2005, 46, 827.
14. Yu, Z. Z.; Yan, C.; Yang, M. S.; Mai, Y. W. Polym Int 2004, 53, 1093.
15. Chen, L.; Phang, I. Y.; Wong, S. C.; Lv, P. F.; Liu, T. X. Mater Manuf Process 2006, 21, 153.
16. Dasari, A.; Yu, Z. Z.; Mai, Y. W. Macromolecules 2007, 40, 123.
17. Cotterell, B.; Chia, J. Y. H.; Hbaieb, K. Eng Fract Mech 2007, 74, 1054.
18. Ou, Y. C.; Yang, F.; Yu, Z. Z. J Polym Sci Part B: Polym Phys 1998, 36, 789.

19. Li, Y.; Yu, J.; Guo, Z. X. Polym Int 2003, 52, 981.
20. Zhou, T. H.; Ruan, W. H.; Rong, M. Z.; Zhang, M. Q.; Mai, Y. L. Adv Mater 2007, 19, 2667.
21. Matonis, V. A.; Small, N. C. Polym Eng Sci 1969, 9, 90.
22. Pukanszky, B.; Tudos, F.; Kolarik, J.; Lednicky, F. Polym Compos 1990, 11, 98.
23. Kolarik, J.; Jancar, J. Polymer 1992, 33, 4961.
24. Stricker, F.; Mulhaupt, R. J Appl Polym Sci 1996, 62, 1799.
25. Hornsby, P. R.; Premphet, K. J Appl Polym Sci 1998, 70, 587.
26. Dubnikova, I. L.; Berezina, S. M.; Antonov, A. V. J Appl Polym Sci 2002, 85, 1911.
27. Liang, J. Z.; Li, R. K. Y.; Tjong, S. C. Polym Eng Sci 2000, 40, 2105.
28. Premphet, K.; Horanont, P. Polymer 2000, 41, 9283.
29. Premphet, K.; Horanont, P. J Appl Polym Sci 2000, 76, 1929.
30. Zhang, L.; Wang, Z. H.; Huang, R.; Li, L. B.; Zhang, X. Y. J Mater Sci 2002, 37, 2615.
31. Premphet-Sirisinha, K.; Preechachon, I. J Appl Polym Sci 2003, 89, 3557.
32. Li, Z.; Guo, S. Y.; Song, W. T.; Hou, B. J Mater Sci 2003, 38, 1793.
33. Yang, H.; Zhang, Q.; Guo, M.; Wang, C.; Du, R. N.; Fu, Q. Polymer 2006, 47, 2106.
34. Yang, H.; Zhang, X. Q.; Qu, C.; Li, B.; Zhang, L. J.; Zhang, Q.; Fu, Q. Polymer 2007, 48, 860.
35. Dasari, A.; Yu, Z. Z.; Mai, Y. W. Polymer 2005, 46, 5986.
36. Tjong, S. C.; Bao, S. P. J Polym Sci Part B: Polym Phys 2005, 43, 585.
37. Chiu, F. C.; Lai, S. M.; Chen, Y. L.; Lee, T. H. Polymer 2005, 46, 11600.
38. Dasari, A.; Yu, Z. Z.; Yang, M. S.; Zhang, Q. X.; Xie, X. L.; Mai, Y. W. Compos Sci Technol 2006, 66, 3097.
39. Gonzalez, I.; Eguiazabal, J. I.; Nazabal, J. Compos Sci Technol 2006, 66, 1833.
40. Gonzalez, I.; Eguiazabal, J. I.; Nazabal, J. Eur Polym J 2006, 42, 2905.
41. Ahn, Y. C.; Paul, D. R. Polymer 2006, 47, 2830.
42. Wong, S. C.; Mai, Y. W. Polymer 1999, 40, 1553.
43. Saint-Michel, F.; Pignon, F.; Magnin, A. J Colloid Interface Sci 2003, 267, 314.
44. Fornes, T. D.; Paul, D. R. Polymer 2003, 44, 3945.
45. Wu, S. H. Polymer 1985, 26, 1855.
46. Wu, S. H. J Appl Polym Sci 1988, 35, 549.
47. Muratoglu, O. K.; Argon, A. S.; Cohen, R. E.; Weinberg, M. Polymer 1995, 36, 921.
48. Wu, L. C.; Chen, P.; Zhang, J.; He, J. S. Polymer 2006, 47, 448.
49. Halpin, J. C.; Kardos, J. L. Polym Eng Sci 1976, 16, 344.
50. Su, X. Q.; Hua, Y. Q.; Qiao, J. L.; Liu, Y. Q.; Zhang, X. H.; Gao, J. M.; Song, Z. H.; Huang, F.; Zhang, M. L. Macromol Mater Eng 2004, 289, 273.
51. Wang, X.; Sun, J.; Huang, R. J Appl Polym Sci 2006, 99, 2268.
52. Hobbs, S. Y.; Bopp, R. C.; Watkins, V. H. Polym Eng Sci 1983, 23, 380.
53. Chen, X. H.; Mai, Y. W. Polym Eng Sci 1998, 38, 1763.
54. Kinloch, A. J.; Young, R. J. Fracture Behaviour of Polymers, 2nd ed.; Elsevier: London, 1985; p 427–428.